Photo-CIDNP studies on reaction centers of rhodobacter sphaeroides

Prakash, Shipra

3 Field dependent photo-CIDNP in reaction centers of *Rhodobacter sphaeroides* R26: A sensitive and precise tool for detection of small changes in electronic structure

---

3.1 Abstract

Photochemically induced dynamic nuclear polarisation (photo-CIDNP) is observed in frozen photosynthetic reaction centers of the carotenoid-less strain R26 of the purple bacteria *Rhodobacter sphaeroides* by ^{13}C solid-state NMR at three different magnetic fields (4.7 T, 9.4 T and 17.6 T). The overall shape of the spectra remains independent of the magnetic field and can be semi-quantitatively explained by simulating spin dynamics in the radical pair state and nuclear relaxation in the donor triplet state. The strongest enhancement is observed at 4.7 Tesla, allowing observation of photo-CIDNP enhanced NMR signals from reaction center cofactors in entire bacterial cells. The correlation of chemical shift in the electronic ground state with the hyperfine interaction in the radical pair and triplet states inherent in this experiment and its high sensitivity allow for the detection of subtle changes in the electronic structure.

3.2 Introduction

Photochemically induced dynamic nuclear polarization (photo-CIDNP) is a method to increase NMR intensities by induction of photochemical reactions, which shuffle the nuclear spin system out of its Boltzmann equilibrium. In contrast to optical pumping, photo-CIDNP does not require polarized radiation. Photo-CIDNP in solution NMR is explained by the radical-pair mechanism where nuclei in singlet and triplet radical pairs gain opposite polarization (Hore and Broadhurst, 1993; Goez, 1997). They can later be observed separately as the radicals diffuse apart and, depending on their spin state, meet a different chemical fate (Closs and Closs, 1969; Kaptein and Oosterhoff, 1969). This mechanism is not feasible in the solid-state for lack of diffusion and not observable for cyclic reactions where the opposite polarization cancels. In solids, photo-CIDNP can be observed by magic-angle spinning (MAS) NMR, a method which overcomes line-broadening due to chemical shift anisotropy (CSA) in solids and allows for detailed analysis of structure, dynamics and functional mechanisms of membrane-bound protein systems (de Groot, 2000; Laws et al., 2002).

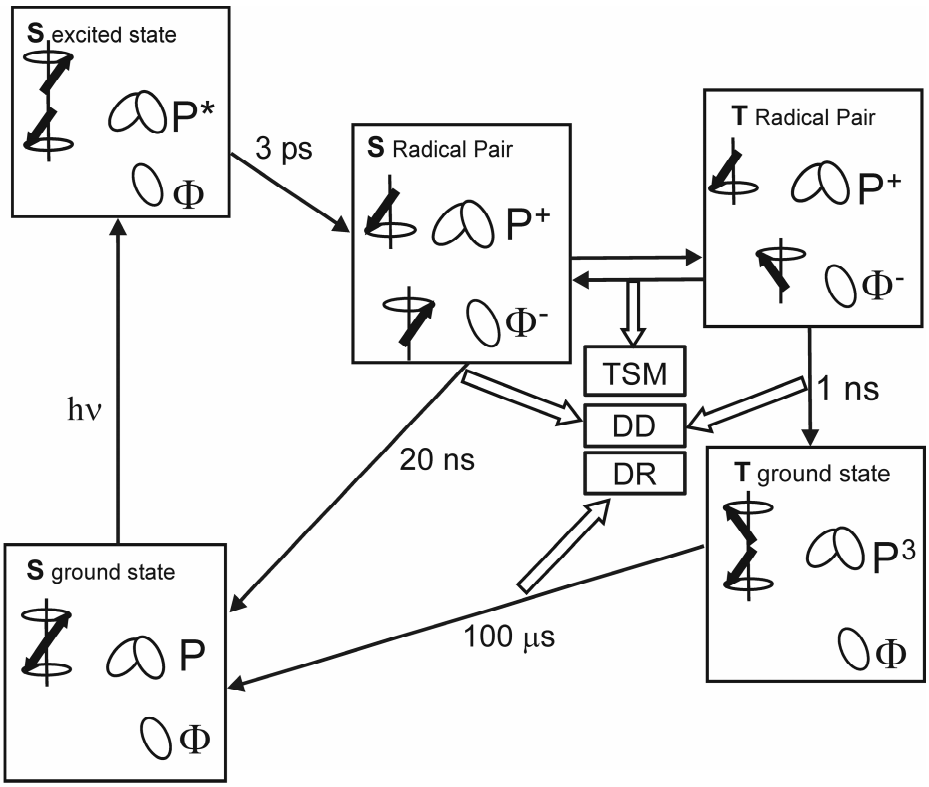

Figure 3.1. Reaction cycle in quinone blocked bacterial RCs. After light-induced electron transfer from the primary donor (P) to the bacteriopheophytin (ϕ), an electron polarized singlet radical pair is formed. The electron polarization is transferred to nuclei via three-spin mixing (TSM) within the radical pair and, via differential decay (DD) due to the difference in lifetime of the two radical pair states. Cancellation of incomplete nuclear spin polarization during long-lived donor triplet is by differential relaxation (DR).

In the solid-state, photo-CIDNP has been observed for the first time in quinone blocked frozen reaction centers (RCs) of *Rhodobacter (Rb.) sphaeroides* R26 and WT under continuous illumination with white light (Zysmilich and McDermott, 1994, 1996b, 1996a; Matysik et al., 2000b; Matysik et al., 2001a; Schulten et al., 2002) (Chapter 2). Photo-CIDNP has not only been observed in bacterial RCs, but in plant photosystems I and II as well (Matysik et al., 2000a; Alia et al., 2004b; Diller et al., 2005).

Upon photochemical excitation of the primary electron donor P, which in RCs of purple bacteria is a BChl dimer composed of P_L and P_M, an electron is emitted to the primary acceptor, a bacteriopheophytin (BPhe) molecule Φ, forming an electron-polarised singlet radical pair (Figure 3.1). In quinone-reduced or depleted RCs, further electron transfer is blocked. Therefore, the singlet radical pair can either relax to the electronic ground state or, depending on the strength of the applied magnetic field, is transferred to a triplet radical pair. The triplet radical pair recombines to a special pair triplet ^3P and an acceptor singlet. Finally, the donor triplet also relaxes to the singlet ground state, so that the entire process is cyclic and opposite polarization originating from singlet and triplet spin-correlated radical pairs cancels.

If the nuclear spin relaxation is significant during the lifetime of the triplet state, this cancellation is not complete (Hore and Kaptein, 1982). Such differential relaxation (DR) was predicted for photosynthetic RCs and later invoked as explanation for the first experimental solid-state photo-CIDNP results (Goldstein and Boxer, 1989; McDermott et al., 1998). However, the DR mechanism could not explain the observed signals from the bacteriopheophytin acceptor, which does not undergo intersystem crossing, and from wild type RCs with a triplet lifetime that is three orders of magnitude shorter. Photo-CIDNP in solids has thus been explained by the simultaneous action of two other mechanisms (Jeschke and Matysik, 2003). In the electron-electron-nuclear three-spin mixing (TSM) mechanism, net nuclear polarization is created in the spin-correlated radical pair due to the presence of both anisotropic hyperfine interaction and coupling between the two electron spins (Jeschke, 1998). In the Differential Decay (DD) mechanism, a net photo-CIDNP effect is caused by anisotropic hyperfine coupling without an explicit requirement for electron-electron coupling if spin-correlated radical pairs have different lifetimes in their singlet and triplet states (Polenova and McDermott, 1999). Based on this approach of two parallel mechanisms, we have been able to explain the ^{13}C photo-CIDNP spectrum of WT RCs, which shows entirely emissive photo-CIDNP signals (Chapter 2). However, in RCs of the carotenoidless R26 strain, having a long lifetime of the donor triplet, the donor signals appear enhanced absorptive. This raises the question whether the DR mechanism is operative in the carotenoidless strain in addition to the two other mechanisms. This Chapter examines this question and, based on the understanding of the origin of the polarization patterns, discusses subtle differences in the electronic structure of the radical pair between RCs of the WT and R26 strains as well as between isolated RCs and whole cells of the R26 strain.

3.3 Materials and Methods

3.3.1 Sample Preparation

The reaction centers (RCs) from *Rb. sphaeroides* R26 were isolated by the procedure of Feher and Okamura (Feher and Okamura, 1978). The removal of Q_A has been done by incubating the RCs at a concentration of 0.6 μM in 4% LDAO, 10 mM o-phenanthroline, 10 mM Tris buffer, pH 8.0, for 6 h at 26 °C, followed by washing with 0.5 M NaCl in 10 mM Tris buffer, pH 8.0, containing 0.025% LDAO and 1 mM EDTA (Okamura et al., 1975). Approximately 5 mg of the RC protein complex embedded in LDAO micelles was used for NMR measurements.

The cells were harvested and suspended in Tris buffer. 70 μL of this cell suspension was used for the experiment. The RCs in the cells were reduced with 0.05 M sodium dithionite in Tris buffer prior to experiments.

3.3.2 MAS-NMR Measurements

The NMR experiments at different fields were performed with DSX-750, DMX-400 and DMX-200 NMR spectrometers equipped with magic angle spinning (MAS) probes. The sample was loaded into a clear 4-mm sapphire rotor and inserted into the MAS probe. The sample was frozen slowly at a low spinning frequency of ν_r = 400 Hz to ensure a homogenous sample distribution against the rotor wall (Fischer et al., 1992). The light and dark spectra were collected with a Hahn echo pulse sequence and TPPM proton decoupling (Bennett et al., 1995). ^{13}C MAS NMR spectra were obtained at a temperature of 223 K under continuous illumination with white light (Matysik et al., 2000b). The rotational frequency for MAS was 8 kHz. For the three fields of 4.7, 9.6 and 17.6 Tesla, a line broadening of 20 Hz, 50 Hz and 120 Hz, respectively, was applied prior to Fourier transformation. In all cases, a cycle delay of 4 s was used. All the ^{13}C-MAS NMR spectra were referenced to the ^{13}COOH response of solid tyrosine•HCl at 172.1 ppm.

3.3.3 Concentration of special pair BChl molecules

Optical density of the sample at 865 nm has been determined to be 1.28. Using an absorbtion coefficient of 75 $mM^{-1}cm^{-1}$ and a ratio of special pair BChls to all BChl *a* cofactors of 2:300 a sample concentration of ~100 nM has been calculated (Hu et al., 2002).

3.3.4 Simulations

Simulations of the coherent spin evolution in the radical pair state and Density Functional Theory (DFT) computations of hyperfine couplings for the triplet state of the special pair donor were performed as described in Chapter 2. The hyperfine anisotropy ΔA of individual carbon nuclei was calculated from the DFT-computed eigenvalues A_{xx}, A_{yy}, and A_{zz} of the hyperfine tensor as $\Delta A = A_{zz}-(A_{xx}+A_{yy})/2$, where A_{zz} is the eigenvalue whose absolute value is maximum. Polarization originating from singlet and triplet pairs was stored separately. Nuclear spin relaxation in the triplet state was taken into account on the basis of Solomon theory by multiplying triplet polarization with a decay factor $\exp(-C\,\Delta A^2\,T_T)$, where T_T is the lifetime of the special pair triplet (Solomon, 1955). The fit parameter C takes the same value for all ^{13}C nuclei within the same spectrum but may vary with magnetic field.

3.4 Results and discussion

3.4.1 Polarization pattern for the R26 strain

The photo-CIDNP spectrum of R26 RCs (Figure 3.2A) exhibits peaks at very similar chemical shifts as the one from WT RCs (Figure 3.2B). However, signals at chemical shifts larger than 135 ppm are absorptive for R26 in agreement with previous work, whereas the whole spectrum is emissive for WT (Zysmilich and McDermott, 1994, 1996b, 1996a; Matysik et al., 2000b). The magnetic field dependence has been measured in dark (Figure 3.3) and in

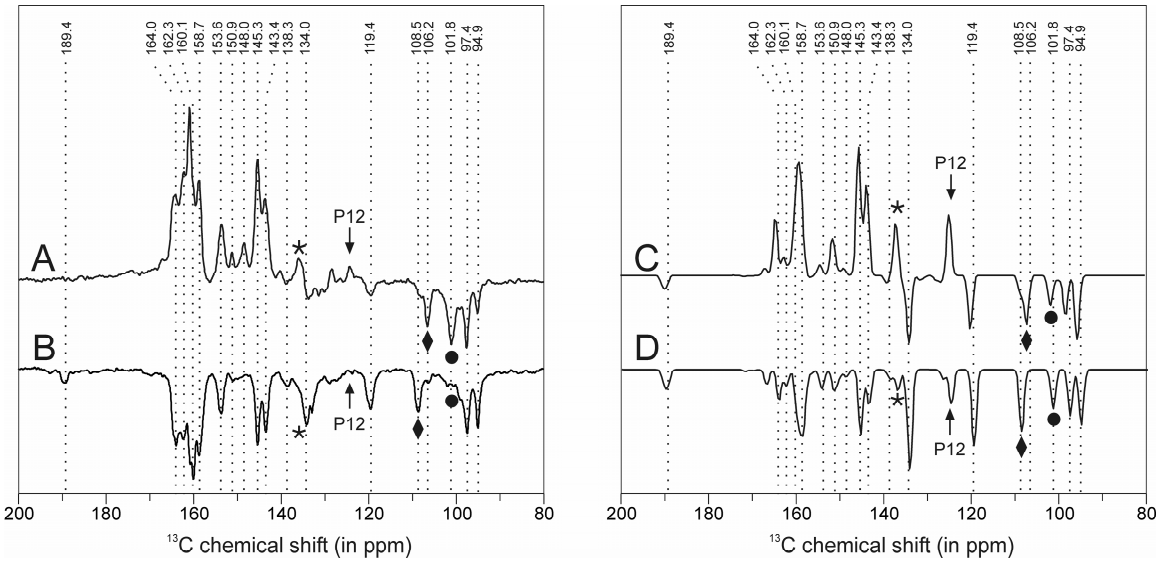

Figure 3.2. ^{13}C photo-CIDNP MAS NMR spectra of RCs of *Rb. sphaeroides* at 223 K and a field strength of 4.7 T. Arrows, asterisks, diamonds, and full circles denote signals that appear to be sensitive to the environment of the RCs and are discussed in the text. Experimental spectrum of (A) R26 RCs and (B) WT RCs. Simulated spectrum of (C) R26 RCs, assuming a lifetime of 100 µs for the triplet state of the special pair. (D) WT RCs assuming a lifetime of 100 ns for the triplet state of the pair.

light (Figure 3.4) for R26 at A: 17.6 T (750 MHz), B: 9.4 T (400 MHz) and C: 4.7 T (200 MHz). For WT, the field dependence has been reported in Chapter 2. This general photo-CIDNP pattern persists at all magnetic fields where the spectra were studied. Our previous assignment (Chapter 2) suggests that the sign change is restricted to signals from ^{13}C nuclei of the special pair. Indeed a simulation including the DR mechanism reproduces the sign change in this range of chemical shifts (Figure 3.2C, D) assuming $C = 4 \cdot 10^{-11}$ s and triplet lifetimes of 100 µs for R26 RCs. We have tested the plausibility of the only fit parameter C by computing the longitudinal relaxation time T_1 for a hypothetic ^{13}C nucleus that is 5 Å away from a paramagnetic center with the same C value (ΔA = 159 kHz). We find T_1 = 0.99 s, which appears reasonable. The fast decay of polarization of some nuclei in the triplet state of the special pair is due to anisotropic hyperfine couplings of the order of 10 MHz. These large couplings are in turn caused by substantial spin density of up to 11.4% in p orbitals on these carbon atoms. The simulations also reproduce the field dependence of the polarization (Figure 3.5), with C values corresponding to T_1 = 0.66 s at 9.4 T and 0.40 s at 17.6 T for a hypothetical ^{13}C nucleus 5 Å away from the paramagnetic center.

In both, WT and R26 centers, the relative peak intensities are only roughly reproduced by the simulations (compare Figure 3.2A, B with C, D). This is not unexpected, as experimental values like the exchange coupling between the two electron spins in the pair as well as life times of singlet and triplet radical pairs and DFT-computed values, such as the ^{13}C hyperfine couplings can well deviate by 20-30% from right values. The only deviation that appears

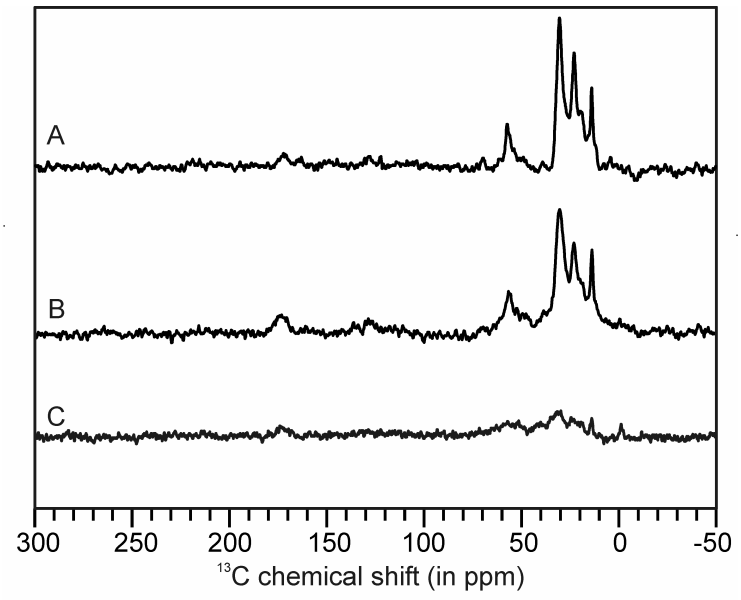

Figure 3.3. ^{13}C MAS NMR spectra of quinone-depleted RCs of *Rb. sphaeroides* obtained at 223 K in the dark at different magnetic fields of 17.6 T (A), 9.4 T (B) and 4.7 T (C).

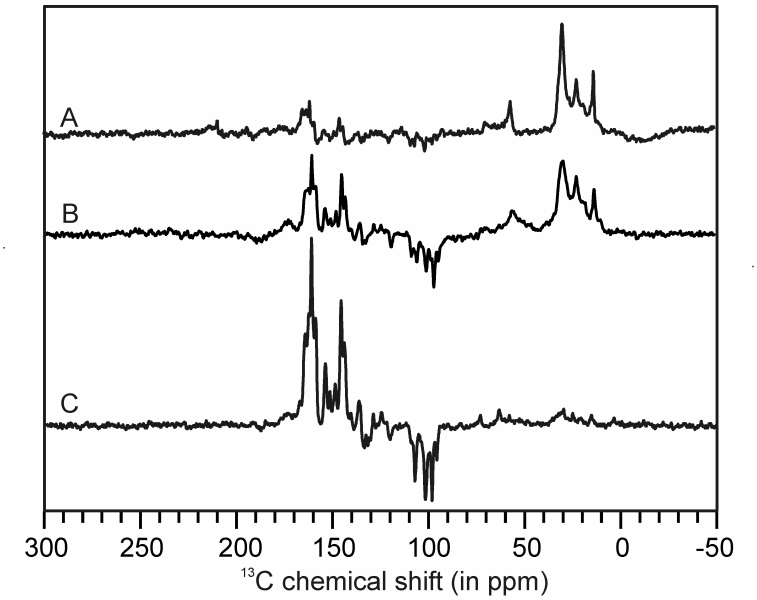

Figure 3.4. ^{13}C MAS NMR spectra of quinone-depleted RCs of Rb. sphaeroides obtained at 223 K under illumination with continuous white light at different magnetic fields of 17.6 T (A), 9.4 T (B) and 4.7 T (C).

really significant is the substantial polarization of the ^{13}C nucleus C-L12/ C-M12 that is predicted by the simulations for both WT and R26 centers, whereas only a weak emissive signal in R26 RCs is observed experimentally at 124.6 ppm (arrows in Figure 3.2). Interestingly, earlier ENDOR and special TRIPLE measurements have detected a sizeable isotropic proton hyperfine coupling for the methyl group attached to this carbon atom (Lendzian et al., 1993; Lubitz et al., 2002). This coupling changes strongly when His M202,

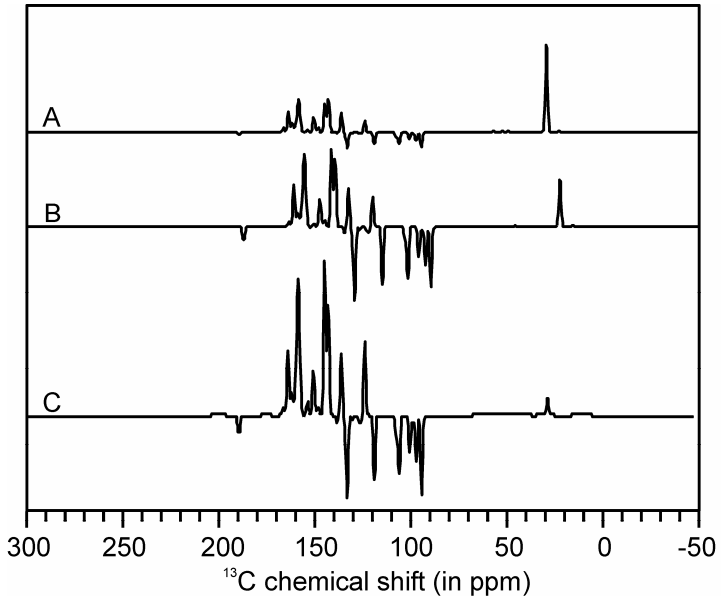

Figure 3.5. Simulated ^{13}C MAS NMR spectra of RCs of *Rb. sphaeroides* strain R26 at different magnetic fields assuming a lifetime of 100 μs for the triplet state of the special pair. The magnetic fields are 17.6 T (A), 9.4 T (B) and 4.7 T (C).

which is directly coordinated to the special pair, is mutated to Leu or Glu. The unexpectedly low photo-CIDNP intensity at position C-L12/ C-M12 may thus indicate an influence of the protein environment on the spin density distribution that is not accounted for in the simplified model of the RC used in our DFT computations.

3.4.2 Implications for the interpretation of solid-state photo-CIDNP spectra

The broad agreement of the photo-CIDNP patterns and their field dependence between experiment and *ab initio* simulations for both WT and R26 RCs lends confidence to the notion that a combination of the DR, TSM, and DD mechanisms is responsible for the non-equilibrium nuclear polarization. In addition, it supports our previous chemical shift assignments (Table 3.1) that were based on results from 2D NMR and DFT computations of chemical shifts by others and ourselves (Facelli, 1998), (Schulten et al., 2002) (Chapter 2 and 4). We may thus interpret the polarization pattern of WT RCs in terms of the spin density distribution in the radical pair state and the polarization change between the WT and R26 spectra in terms of the spin density distribution in the triplet state of the donor. To do so, we note that for all three mechanisms the polarization of a given ^{13}C nucleus is roughly proportional to the square of the anisotropic hyperfine coupling of that nucleus. The technique is thus particularly sensitive to spin density in p orbitals. For instance, the ^{13}C with a shift of 136.8 ppm (asterisks in Figure 3.2), assigned to C-L4 in the special pair, has a higher spin density in its p orbital in the triplet state than in the radical pair state, according to both experiment (Figure 3.2A, B) and simulation (Figure 3.2C, D).

Cofactor carbon no	photo-CIDNP WT[a]	photo-CIDNP R26[b]
Φ13[1]	189.4	-
L6	164.0	164.4 A
M19	162.3	162.5 A
M14	160.1	161.0 A
L9, M9	158.7	158.8 A
M16	150.9	151.3 A
L11	153.6	153.7 A
M1	-	148.6 A
L16	145.3	145.6 A
M2	143.4	143.8 A
Φ1, Φ3	138.3	138.8 E
L4	-	136.8 A
Φ2	134.0	133.7 E
L12, M12	-	124.6 A
Φ12	119.4	119.7 E
Φ15	108.5	106.8 E
Φ10	-	101.3 E
Φ5	97.4	97.8 E
Φ20	94.9	95.2 E

A = absorptive, E = emissive.
[a] (Schulten et al., 2002), Chapters 2 and 4
[b] This work

Table 3.1. Tentative assignments of the ^{13}C photo-CIDNP NMR signals.

The high sensitivity of chemical shifts to changes in the electronic structure of the ground state allows for a detailed comparison of WT and R26 RCs. Two remarkable changes are apparent in Figure 3.2A, B. First, a strong peak is detected at 108.5 ppm in WT (♦) and a weak peak at 106.2 ppm, while in R26 the ratio is inverted. This peak is assigned to the acceptor nucleus C-Φ15. Possibly, the difference may be due to different states of the protein pocket from which the quinone has been removed (see below). Second, the peak at 101.8 ppm that is predicted for both WT and R26 centers is actually observed only in R26 (●). This peak is assigned to the acceptor nucleus C-Φ10, for which a strong signal has been calculated (Figure 2D). Therefore, the absence of this signal in Figure 3.2B indicates a disturbed environment, which may be due to the empty quinone pocket, while this pocket may be refilled with a substituting molecule maintaining the structure in Figure 3.2A.

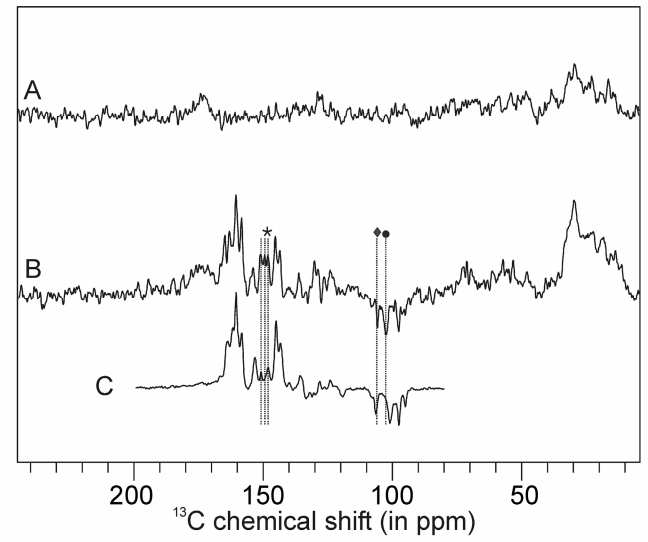

Figure 3.5. ^{13}C solid-state MAS NMR spectra of intact *Rb. sphaeroides* R26 cells at a field strength of 4.7 T and spinning frequency of 8 kHz in (A) dark, (B) light and RCs in (C) light.

3.4.3 Nanomolar concentrations probed in intact cells

The strong photo-CIDNP enhancement at a field strength of 4.7 T enables the study of cofactor molecules in their native cellular environment at a concentration of ~100 nM without isotope enrichment. The dark spectrum of the intact cells of *Rb. sphaeroides* R26 (Figure 3.5A) shows broad peaks at 173 and 35 ppm. Under illumination (Figure 3.5B) the photo-CIDNP signals from the donor and acceptor appear. The light-induced signals appear in the region from 90 to 170 ppm. The overall photo-CIDNP intensity pattern is similar, but in some respects distinct from the spectrum of isolated reaction centers at 4.7 T (Figure 3.5C). The similarity between the photo-CIDNP spectrum from the isolated RCs and intact cells suggests that the ground state electronic structure of the special pair is not strongly influenced by the surrounding protein complexes in the natural environment of an intact cell. The signals of acceptor nucleus C-Φ15 and C-Φ10 in R26 cells (♦, ●) (quinone-reduced) are observed at 106.1 ppm and 102.3 ppm, in agreement with the isolated R26 RCs (quinone-depleted), suggesting that in isolation the quinone binding site is not disturbed. In the shift range between 148 and 152 ppm, signals that are assigned to C-M1 and C-M16 exhibit significantly stronger absorptive polarization in cells compared to isolated reaction centers. Considering the behavior of the same peaks in isolated RCs of WT and R26 as well as in cells, we can identify position C-M1 and C-M16 as a hot spot, where electron spin density appears to depend strongly on small changes in the environment of the special pair.

In conclusion, photo-CIDNP MAS NMR allows for the selective study of moderately sized molecules in an intact cell at natural abundance (1% ^{13}C). Combination with ^{13}C-isotope labeling is expected to further increase the signal by a factor of 100 to a total enhancement factor of a million. Such a strong polarization source might be used in the near future as a

"spin torch" for illuminating the vicinity of RCs, or their artificial equivalents, by secondary polarization transfer.